nature astronomy

Article

https://doi.org/10.1038/s41550-024-02469-4

Partial differentiation of Europa and implications for the origin of materials in the Jupiter system

Received: 18 April 2023

Accepted: 11 December 2024

Published online: 27 January 2025

Check for updates

Flavio Petricca[1,2] ✉, Julie C. Castillo-Rogez[1], Antonio Genova[2], Mohit Melwani Daswani[1], Marshall J. Styczinski[3], Corey J. Cochrane[1] & Steven D. Vance[1]

The Galileo mission measured the gravity field around Europa. The results indicated that the moon's interior is mostly made of rock (~90 wt%). However, the level of differentiation of the deep interior is still poorly understood. We constrain the interior of Europa using Galileo gravity data and a combination of geophysical and geochemical models that connects the origin of the materials accreted in the Jupiter system with the observed gravity field. The results indicate that Europa is partially differentiated and that it probably formed primarily from CV chondrite material. We investigate this finding by coupling thermal evolution models with a detailed treatment of Fe–FeS melting. The metal–silicate differentiation temperatures (>1,600 K) are not attained if Europa formed about 4 Myr after the production of calcium aluminium inclusions. The leaching of potassium during thermal metamorphism further limits differentiation. Our results imply a cold evolution for Europa and suggest that part of water inventory of Europa was supplied by external sources, possibly by comets. These implications can be tested with the gravity data that will be acquired by Europa Clipper and JUICE.

The interior structure of Europa records key information about its accretional environment and evolution and the potential for a habitable ocean[1–3]. Geophysical constraints have been independently inferred from gravity and magnetic data acquired by the Galileo mission at Europa[4,5]. However, knowledge of the interior structure remains limited, with the largest uncertainties affecting the ice thickness, the ocean depth, the mantle composition, and the state and size of a putative metallic core[6].

An analysis of Galileo radio science data has yielded Europa's mass and moment of inertia (MoI; 0.346 ± 0.005)[4], which have been used to constrain the moon's interior structure (for example, refs. 7,8). Anderson et al.[4] argued that Europa probably experienced advanced differentiation because radiogenic heating alone would be sufficient to segregate the metal into a central core. The quadrupole gravity coefficients J_2 and C_{22} were estimated by fixing their ratio to the value expected for a hydrostatic body ($J_2/C_{22} = 10/3$), and the MoI was derived from C_{22} using the Radau–Darwin approximation[9].

Recently, Gomez Casajus et al.[10] presented an independent analysis of Galileo radio science data and a new estimate of Europa's gravity field, which yielded a considerably higher value of the MoI (0.3547 ± 0.0024) compared to the previous solution[4]. The MoI was still derived with the Radau–Darwin approximation, but an independent solution for J_2 and C_{22} was obtained that confirmed the assumption of hydrostatic equilibrium, although within large error bars. Additionally, the recent analysis was carried out by processing a larger dataset with a refined calibration of the effects of Earth's troposphere and ionosphere

[1]Jet Propulsion Laboratory, California Institute of Technology, Pasadena, CA, USA. [2]Department of Mechanical and Aerospace Engineering, Sapienza University of Rome, Rome, Italy. [3]Blue Marble Space Institute of Science, Seattle, WA, USA. ✉e-mail: flavio.petricca@jpl.nasa.gov

https://doi.org/10.1038/s41550-024-02469-4

Table 1 | Free parameters varied in the MCMC inversion of the interior structure

Moon	Parameter	Units	Step	Range
Europa	Core radius	km	20	0–1,000
	Core density	$kg\,m^{-3}$	50	5,150–8,000
	Ocean depth	km	5	0–200
	Ocean density	$kg\,m^{-3}$	5	1,000–1,200
	Ice-shell thickness	km	5	0–200
Ganymede	Core radius	km	50	0–1,500
	Core density	$kg\,m^{-3}$	50	5,150–8,000
	Mantle density	$kg\,m^{-3}$	25	2,500–4,500
	HP ice-layer thickness	km	25	0–800
	HP ice-layer density	$kg\,m^{-3}$	5	1,200–1,400
	Water-ice I shell thickness	km	25	0–800
	Water-ice I shell density	$kg\,m^{-3}$	10	800–1,200

The parameters were bounded to prevent the generation of physically inconsistent models.

Table 2 | Hydrosphere thickness and water mass relative to the total mass derived for different compositions

Primordial composition	Hydrosphere thickness (km)	Relative water mass (wt%)
MC-scale	128^{+7}_{-3}	$7.4^{+1.3}_{-0.4}$
CI	88^{+6}_{-4}	$5.1^{+0.7}_{-0.4}$
CM	78^{+6}_{-4}	$4.5^{+0.9}_{-0.4}$
67P/C–G D/I = 6:1	28^{+6}_{-5}	$1.8^{+0.4}_{-0.5}$
67P/C–G D/I = 4:1	25^{+7}_{-5}	$1.6^{+0.5}_{-0.4}$

The only inversion that provided posterior properties in line with expectations (7.0–9.0 wt%) was the inversion based on the MC-scale model.

on the radiometric data and an improved knowledge of the Jupiter system dynamics, including an updated gravity field and ephemerides.

The significantly larger MoI implies a less differentiated interior structure and challenges the inference that Europa has a differentiated metallic core based on the older value of the MoI. To investigate the implications of the new measurement for Europa's deep interior, we combined geophysical and geochemical modelling of the interior with thermal evolution models. The deep interior structure is characterized by a Bayesian inversion that uses the mass and MoI derived from Galileo data as constraints. This technique enables the determination of interior models that are consistent with the observations. The relevant interior properties are treated as free parameters, for which we generated probability distributions. The Bayesian analysis was then extended to Ganymede to assess whether the interior properties derived are consistent with the composition inferred for Europa, as would be expected for satellites that accreted in the same protoplanetary nebula. The interior structure was retrieved from the inversion of the measured gravity field, which was derived from a combination of Galileo and Juno radio science data[11].

Results

Inversion of the interior structure

Our inversion of the interior properties of Europa and Ganymede was performed with a Markov chain Monte Carlo (MCMC) method (for example, see refs. 12–14) to retrieve the interior properties in agreement with the mass and MoI[4,10] by accounting for the credible intervals associated with their measurement uncertainty. The parameter spaces (Table 1) describing the interiors of both moons were explored by using random walkers to perturb each free parameter and map the observed mass and MoI. The resulting probability distributions are reported in terms of central value, selected as its mode, and 1-standard-deviation-level (~68% of output models) credible intervals, determined through the highest posterior density method (for example, see ref. 15).

Deep interiors of Europa and Ganymede. The existence of a metallic core within Europa has not been definitely established from gravity data. However, its existence has been advocated on the grounds that radiogenic heating alone in the deep interior would be sufficient to promote partial melting of the silicates and separation of a denser metal-rich phase[4,6]. Trinh et al.[16] argued that Europa followed a colder evolutionary pathway. Metallic alloy melting in the mantle could have been slowed or prevented by some combination of slow accretion, insufficient suppression of the melting point of iron by sulfur and other materials, and loss of heat as the rocks dehydrated. The metallic core would have formed billions of years after accretion or not at all.

The objective of our study was to constrain the properties of the deep interior. Our methodology is outlined in Supplementary Fig. 1. We generated interior models by assuming a multi-layer structure for the rocky mantle. The other layers were described by uniform properties. We explored a broad range for the core radius (0–1,000 km) in the MCMC framework. By integrating geochemical modelling into our inversion framework, we built a radial profile for the temperature, pressure and density of the mantle for an assumed primordial composition ('Modelling Europa's interior' in Methods and Supplementary Figs. 2 and 3). The reference temperature profile used to build the mantle model was based on the output of thermal evolution models that are consistent with geochemical models in terms of radioisotope content and thermophysical properties (Supplementary Information Section 1).

For the rocky mantle, we considered three chondritic compositions based on Melwani Daswani et al.[17] (CM, CI and MC-scale) and two cometary compositions based on comet 67P/Churyumov–Gerasimenko (67P/C–G) with a dust-to-ice mass ratio (D/I) equal to 4 or 6 (Supplementary Table 1)[18]. The MC-scale composition was derived from a Monte Carlo model that scaled the likelihood of Europa's building blocks around Jupiter according to their distribution in the early Solar System[19], resulting in a composition dominated by CV chondrite material. The evolution of the density of the materials as a function of temperature and pressure was tracked with Perple_X (Supplementary Fig. 4)[20,21], which introduced a constraint on the density of the mantle. Further analyses were performed with a uniform mantle to check the consistency with the inversions based on a multi-layer mantle (Supplementary Information Sections 2 and 3 and Supplementary Figs. 5–7).

The joint inversion of gravity and compositional models enabled us to fit of the observations with all the assumed primordial compositions. To determine the composition that best represents Europa's building blocks, we analysed the inferred hydrosphere thickness, which yielded the total water mass. Because each composition model led to a different density for the multi-layer mantle, the hydrosphere thickness resulting from each inversion was different, with lower mantle densities corresponding to thinner hydrospheres. Previous investigations of Europa's interior structure found hydrosphere thicknesses in the range 120–150 km, corresponding to a water fraction between 7.0 and 9.0 wt% (refs. 6,7). We assessed each composition by comparing the water mass derived from our inversion with this expected range. Table 2 provides the hydrosphere thickness and water mass relative to Europa's total mass for each composition. Figure 1 shows the relative water mass posterior probability. Owing to the low rock density

https://doi.org/10.1038/s41550-024-02469-4

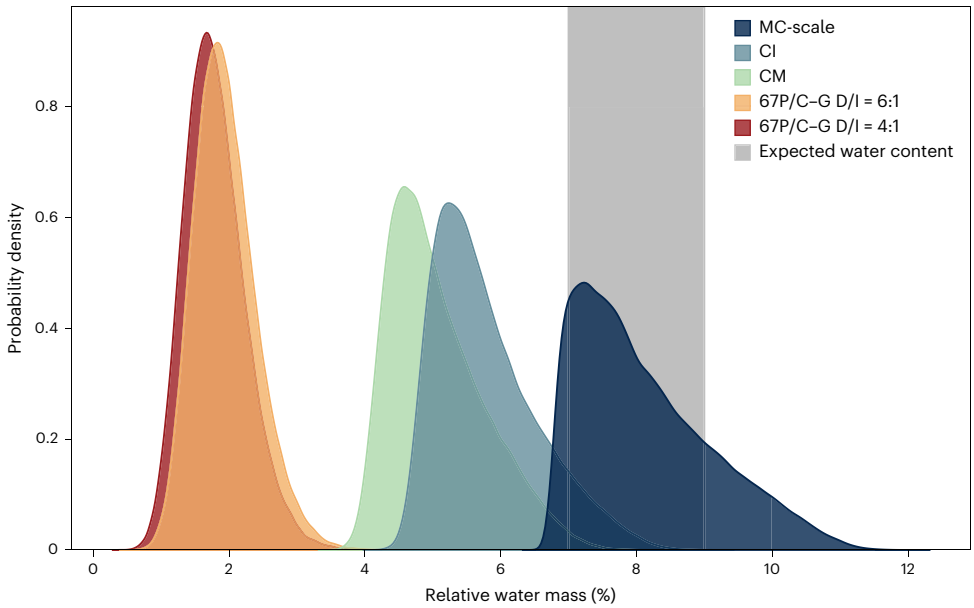

Fig. 1 | Percentage of water mass relative to Europa's mass derived from our inversion for each composition. The grey shaded area is the expected water content of Europa (7.0–9.0 wt%)[6,7,17]. The only primordial composition that yields a present-day water mass fraction that could probably match this range is the MC-scale model (blue), which comprises a large amount of CV chondrite material. The compositions based on CI (azure), CM (teal) chondrites and comet 67P/C–G with D/I = 6 (orange) or 4 (red) yielded substantially lower water mass fractions.

(~2,750 kg m^{-3}; Supplementary Fig. 3), the inversion based on cometary compositions required a thin hydrosphere (25^{+7}_{-5} km and 28^{+6}_{-5} km for D/I = 4 and 6, respectively) to match the gravity data, constraining the water mass fraction to only $1.6^{+0.5}_{-0.4}$ wt% and $1.8^{+0.4}_{-0.5}$ wt%. Similarly, inverting the CM and CI compositions yielded relatively thin hydrospheres, with thicknesses of 78^{+6}_{-4} km and 88^{+6}_{-4} km, respectively. The water content was correspondingly small ($4.5^{+0.9}_{-0.4}$ wt% and $5.1^{+0.7}_{-0.4}$ wt%). Only the inversion based on the MC-scale model produced a reasonable hydrosphere structure, with an inferred hydrosphere thickness of 128^{+7}_{-3} km and a corresponding present-day water fraction of $7.4^{+1.3}_{-0.4}$ wt%.

By using this model to build the multi-layer mantle structure, the inversion yielded significant differences between the deep interior structures derived from the two MoI values (Fig. 2). Although the older MoI value required a relatively large metallic core with radius 425^{+103}_{-134} km, models constrained by the recent value are consistent with a partially differentiated Europa or a small metallic core, with radius in the range 49–269 km.

We extended our Bayesian analysis to Ganymede to test whether the MC-scale composition is also consistent with its interior structure. Gravity data from Galileo have been interpreted as evidence of a metallic core with a radius in the range 400–1,300 km (for example, refs. 7,22). Further evidence was provided by Galileo magnetometer measurements of an intrinsic magnetic field[23], which can probably be explained by an internal dynamo generated in a metallic core[24,25]. We explored models consistent with a wide space of core configurations, with the radius varying in the range 0–1,500 km. A high-pressure (HP) ice layer and a water-ice I shell were included in the modelling ('Modelling Ganymede's interior' in Methods and Table 1). We constrained our modelling of Ganymede with the mass and MoI from Galileo data only (0.3105 ± 0.0028)[22] and with a combination of Galileo and Juno data (0.3159 ± 0.0052)[11]. The larger MoI derived from the combination of Galileo and Juno gravity data yielded a slightly less differentiated interior (core radius within 175–815 km), whereas the older MoI indicates radii in the range 225–900 km (Fig. 3). In both cases, the gravity data are consistent with a broad range of configurations for the deep interior, including cores smaller than previously suggested. The mantle density is constrained to the ranges 2,906–3,630 kg m^{-3} and 3,054–3,892 kg m^{-3} by the recent and older MoI estimates, respectively (Fig. 3). Although less precisely determined than for Europa, the retrieved rock density for Ganymede is consistent with the bulk density of Io (3,527 kg m^{-3})[26] and with an inferred primordial composition like that in the model proposed for Europa.

Discussion

The combination of our geophysical and geochemical models introduces a connection between Europa's origins and current state that allowed us to narrow down the possible origin of the moon's materials and thermal evolution. Based on the results of our inversion, the only composition model that yielded a reasonable hydrosphere volume and that could explain a cold evolution of Europa is the MC-scale model. Being largely dominated by CV chondrites, this model is also consistent with the expected material distribution in the early solar nebula, which supports that the CM and CV chondrite parent bodies were present in Jupiter's vicinity (for example, refs. 17,19).

The primordial composition constrains the total amount of water available to form the hydrosphere. Therefore, we compared our results to the water mass contained in the building blocks of Europa predicted by cosmochemical constraints, that is, the mass of water that can be sourced to the hydrosphere by the mantle rocks during thermal metamorphism. Assuming that all the primordial hydrogen reacts to form water that is released during metamorphism, the amount of water predicted for cometary compositions is 26.6 wt% and 18.6 wt% for D/I = 4 and 6, respectively. Similarly, metamorphic fluids released by CM- and CI-based minerals would provide 13.5 wt% and 17.6 wt% of Europa's mass, respectively. In all these cases, the present-day water mass that we inferred (Table 2) is significantly smaller than the water devolatilized from the interior. Invoking a water-loss mechanism to reconcile these estimates is challenging. Mass ejection through plumes could release up to 24 wt% of the total ocean mass to space[17], which, thus, only partially explains the loss of volatiles. Furthermore, this result was obtained under optimistic assumptions on the efficiency of water delivery. On the other hand, the amount of fluids extracted through thermal metamorphism in the MC-scale model (2.6 wt%) is insufficient to produce Europa's current water mass. The initial inventory of water could be supplemented by the outward diffusion

https://doi.org/10.1038/s41550-024-02469-4

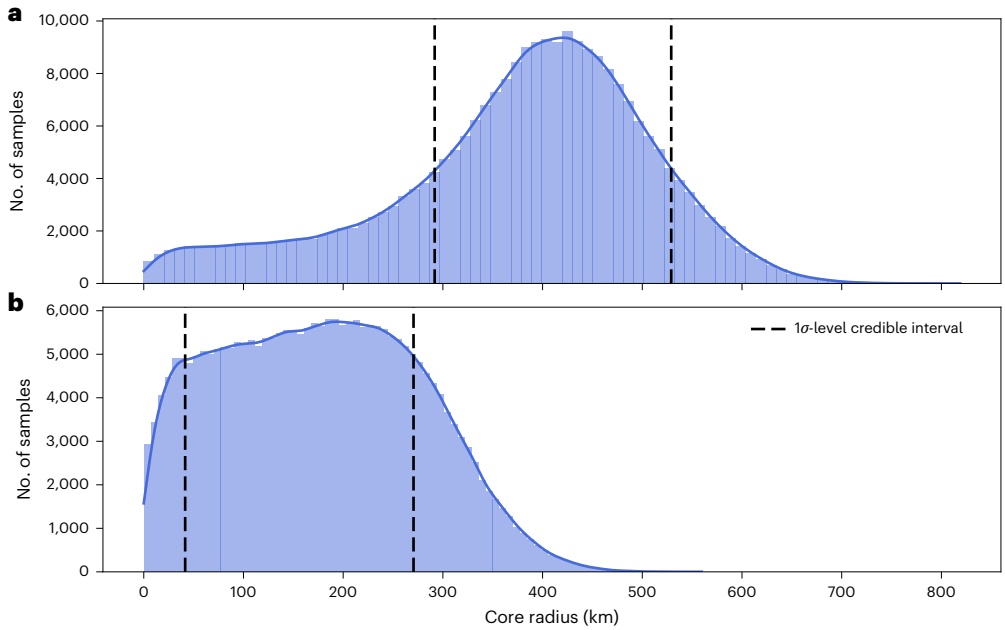

Fig. 2 | Histograms of Europa's core radius obtained by constraining the inversion with two different MoIs. a, MoI derived by Anderson et al.[4]. **b**, MoI derived by Gomez Casajus et al.[10]. Each sample in the histograms corresponds to a model generated in the Bayesian inversion. The mantle structure was determined by assuming a temperature profile from the output of thermal evolution modelling and the starting composition from which Europa accreted, here assumed to be given by the MC-scale model, which is dominated by CV-type materials. The older MoI requires a relatively large metallic core (radius of 425^{+103}_{-134} km). Models constrained by the more recent MoI are consistent with a partially differentiated Europa or a small metallic core, with a radius in the range 49–269 km.

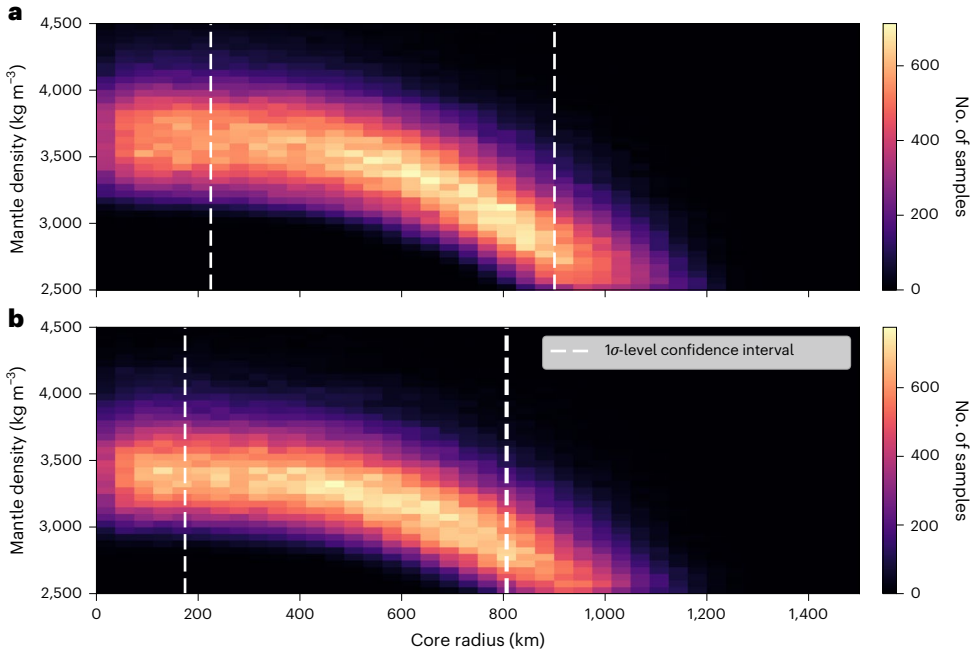

Fig. 3 | Histograms for mantle density and core radius of Ganymede, obtained by constraining the inversion with different MoIs. a,**b**, MoIs are from the analyses of Galileo radio science data (**a**)[22] and a combination of Galileo and Juno radio science data (**b**)[11]. The histograms are colour-coded according to the number of samples. Each sample corresponds to a model generated in the Bayesian inversion. The more recent MoI yielded a less differentiated interior, with the core radius probably in the range 175–815 km and with an average mantle density of 2,906–3,630 kg m^{-3}. The older MoI yielded a core radius in the range 225–900 km and a mantle density of 3,054–3,892 kg m^{-3}.

and condensation of water vapour released by the dehydration of the chondritic particles that populated the Jovian circumplanetary disk, as proposed by Mousis et al.[27]. This scenario predicts that the Galilean moons accreted from the same ice-depleted building blocks and produces the observed water content gradient[27]. An alternative possibility is that, as suggested by Melwani Daswani et al.[17], the other volatiles could be supplied by the late delivery of cometary material (~5.0–6.0 wt%).

https://doi.org/10.1038/s41550-024-02469-4

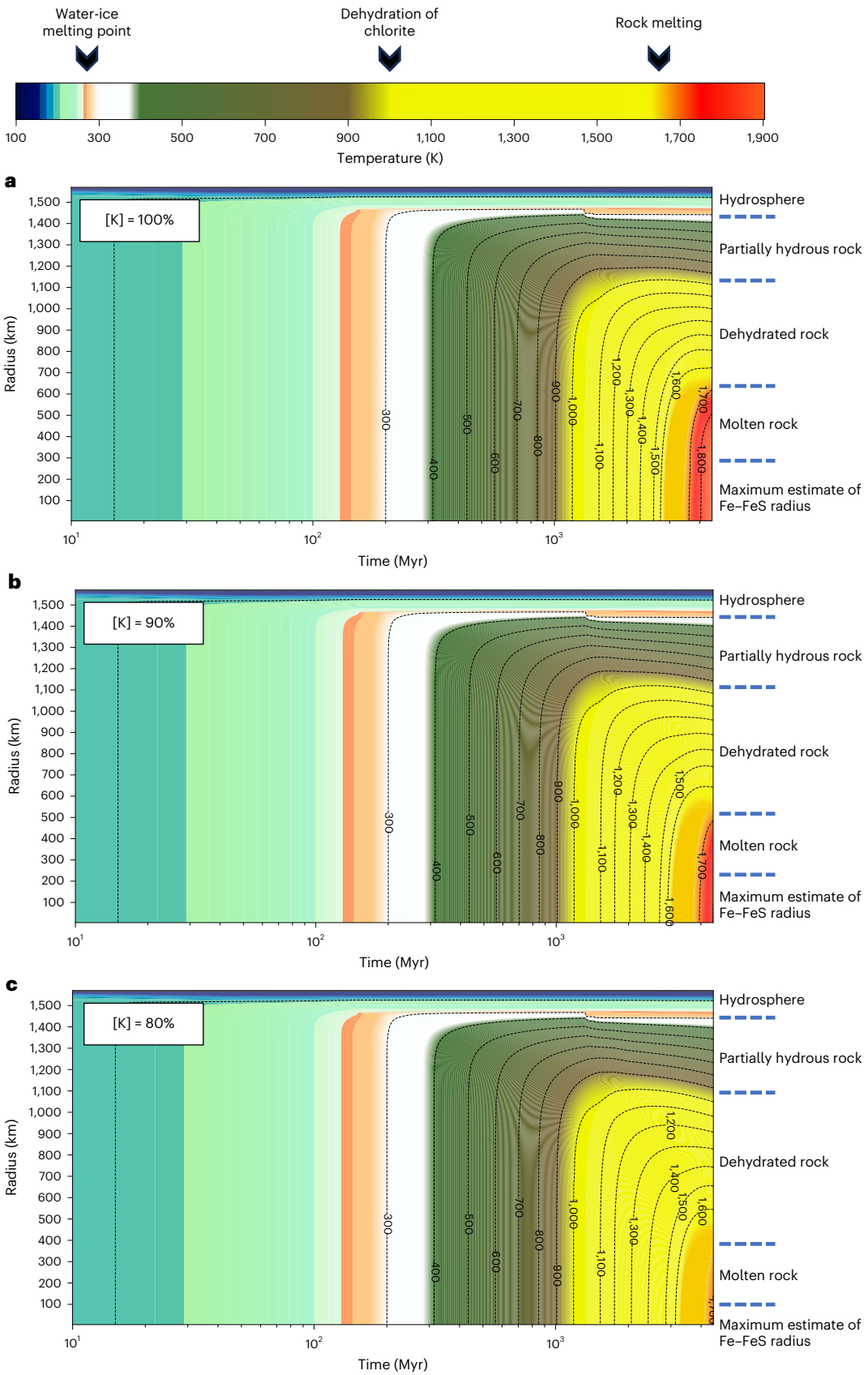

Fig. 4 | Thermal evolution models of Europa assuming a MC-scale reference composition. a–**c**, Results are for the time of formation of 4 Myr after CAIs assuming three different weight fractions of potassium leached from the rocks, indicated by [K]: **a**, 0 wt%, **b**, 10 wt% and **c**, 20 wt% potassium leached from the rocks.

The small or potentially absent metallic core for Europa implies a cold mantle evolution. Recent developments in understanding the early history of the Jupiter system and the geochemical modelling of Europa provide a potential explanation for this paradigm change. Europa probably formed late in the evolution of Jupiter's circumplanetary disk. A first generation of moons was probably lost into Jupiter through type I migration. The Galilean moons would have formed towards the end of the circumplanetary disk lifetime, estimated as ~4 Myr (ref. 28). Hence, the contribution of ^{26}Al to Europa's heat budget was probably minor, thus removing a large heat source for early differentiation. Accretional models yield a range of possible starting compositions for the moons. Slow accretion (a few hundred kiloyears) of pebbles or accretion of material within the circumjovian disk could have led to a relatively cool start[29]. Trinh et al.[16] argued that Europa may not by then have formed its metallic core if a slow accretion scenario is combined with other factors, such as a low sulfur content and the dehydration of the rocks. The objective of the thermal evolution models that we introduced is to investigate this cold scenario. The combination with the mineralogical models allowed us to narrow down possible factors that could explain the partially differentiated state. Notably, the initial inventory of potassium in CV chondrites is half that of CI chondrites[30], which many studies have assumed as the reference composition when modelling Europa's thermal evolution. Tracking the evolution of the mantle mineralogy with pressure and temperature, we also accounted for the role of pressure in suppressing melting. Because of the strong pressure dependence of the Fe–FeS eutectic (Supplementary Fig. 8)[31], a metallic core would differentiate at temperatures in excess of 1,700 K in the lower mantle. Furthermore, potassium leaching during an early phase of aqueous alteration and later during a phase of thermal metamorphism could substantially slow the heating of the rock. Thermal metamorphism could theoretically have led to the release of almost the entire potassium content of Europa's rock into the ocean[17]. However, a fraction of the fluids probably returned to the host rock during their ascent (metasomatism)[17].

We present in Fig. 4 an example of thermal evolution assuming the MC-scale composition and a time of formation of 4.0 Myr with respect to calcium- and aluminium-rich inclusions (CAIs). Our thermal evolution modelling assumed conductive heat transfer, with radiogenic and tidal heating as the main heat sources. We modelled the tidal heating based on the computed pressure and temperature and on terrestrial analogues to derive the viscosity and rigidity structures. Using our models, we found that tidal heating becomes significant when the temperature reached 1,600 K below radius 700 km, increasing up to 1×10^{-11} W kg^{-1}, the same order of magnitude as the amount of radiogenic heating at approximately 1.5 Gyr. Therefore, in the cold evolution scenario that we modelled, tides play a limited role during most of the evolution of the mantle but can lead to partial melting of the silicate and differentiation of a small core in the last billion years. The temperatures required to trigger the melting of the metallic alloys are not reached or affect only the inner ~235 km if >10 wt% potassium is leached. We did not track the variations of tidal heating as a function of orbital evolution. The thermal-orbital evolution study by Hussmann and Spohn[32] showed that Europa's eccentricity could have been higher in the past. Accounting for the coupled thermal-orbital evolution could lead to an increase in the tidal heating, with the subsequent formation of a larger metallic core, as shown by Trinh et al.[16]. However, here we focused on evolution scenarios that can reproduce the small or absent metallic core inferred from the gravity observations. Another aspect that could lead to a warmer evolution is an earlier time of formation. Supplementary Fig. 9 shows that the maximum temperature reached in the deep interior could increase by ~100 K when the time of formation is moved earlier by 0.5 Myr.

The results presented in this work also apply to the other Galilean moons. The density range derived for Europa's rock encompasses Io's density and the average value is only 3% above that of Io (Supplementary Information Sections 2 and 3 and Supplementary Fig. 6). Our analysis for Ganymede implies that its bulk composition may also be like that in the model presented for Europa, within the large uncertainty on its composition that we inferred from the gravity data. Previous works suggested that, to match the MoI derived from Galileo data, Ganymede should have accreted a significant amount of organic-rich cometary material[33]. Although our models do not rule out this scenario, note that both MoI values can be explained by high mantle densities, consistent with the accretion of materials with low organic content. The differentiation of a metallic core in Ganymede implies that the temperatures reached in the deep interior during the moon's evolution were higher than those in Europa. A hotter evolution of Ganymede's interior has already been addressed following the unexpected finding of its metallic core[24]. We modelled the evolution of Ganymede using the same models applied to Europa. We found that the thicker mantle would support the build-up of a greater amount of heat in comparison to Europa, thus increasing temperatures in the deep interior by up to 200 K, which could be sufficient to drive advanced differentiation. Furthermore, the higher pressure in Ganymede's interior could suppress potassium leaching, retaining a key heat source (Supplementary Section 4). Additionally, Ganymede probably experienced a period of enhanced tidal heating during the evolution into the Laplace resonance[34,35], possibly induced by resonances that affected Ganymede's evolution but that did not strongly involve Europa. An alternative possibility is that the Laplace resonance was established during the formation of the system[36]. Ganymede would not then have experienced intense tidal heating and the divergent evolution of the two moons could be explained only by their different sizes. Refined studies of the coupled thermal-orbital evolution of the Galilean moons and future measurements will help in reducing the uncertainties on the degree of differentiation of the moons, narrowing down possible scenarios of formation and evolution.

If a CV-dominated composition is applicable across the Galilean system, it entails a relatively poor carbon content in the mantle (<1 wt%). As a result, the fraction of carbon compounds released as a consequence of the metamorphism of organic matter and carbonate would be small[17]. However, the addition of cometary material to compensate for the missing hydrosphere volume (MC-scale model) increases the amount of carbonates precipitated in Europa's ocean by a factor 50, from 1.3×10^6 km^3 to 6.9×10^7 km^3 (ref. 17). Finally, our results suggest that Europa's upper mantle is cold and that rock melts deep in its mantle. Hence, volcanic activity at the base of the ocean may be limited.

The methodology developed in this work provides a framework for analysing and interpreting measurements that will be collected by future missions. The Europa Clipper mission is expected to arrive in the Jupiter system in 2030, and it will measure the gravity and magnetic fields near Europa[37,38]. Both gravity and magnetic field measurements may provide a way to test the results presented in this work and settle questions related to the degree of differentiation in the interior of Europa. Gravity measurements will be key to understanding whether Europa is in a hydrostatic state and to improving the estimate of MoI for Europa[37]. Long-period magnetic waves may penetrate Europa's interior and enable a potential assessment of the response of the metallic core to magnetic induction[39]. The combination of gravity and magnetic field measurements could provide evidence for the existence of a metallic core.

Methods

Geophysical constraints

The interior models were generated by adjusting the interior properties to match the measurements used as constraints within their reported uncertainties. Each parameter was randomly initialized by the MCMC algorithm and varied within certain limits that prevented the generation of physically inconsistent models (Table 1). Once a

model was generated, it was evaluated by computing its mass M and its normalized MoI C/MR^2. For a model with N layers, the mass and MoI were computed as:

$$M = \frac{4}{3}\pi \sum_{i=0}^{N} \rho_i \left(r_{i+1}^3 - r_i^3\right), \quad (1)$$

$$C = \frac{8}{15}\pi \sum_{i=0}^{N} \rho_i \left(r_{i+1}^5 - r_i^5\right). \quad (2)$$

where ρ_i is the density of the ith layer and r_i is the radial distance from the center of the interface between the layer i and the layer $i-1$ (r_0 is equal to zero). The mass and normalized MoI were computed for each model and compared to the observations to evaluate the probability of accepting the model.

MCMC algorithm

The inversion of Europa's interior structure was carried out with the MCMC algorithm, which enabled a probabilistic exploration of the moon's interior by generating models that satisfied the constraints given by the geophysical observations[12,13]. The multi-dimensional parameter space was explored with the Metropolis–Hastings sampler[40]. The models were generated sequentially in chains and were evaluated by computing their deviations from the observations to determine whether they could be accepted in the chain or be rejected. A model with random parameters was generated to initialize the algorithm. For each step j of the algorithm and the set of parameters x_j, a proposal distribution $p(x_{j+1}|x_j)$ was formulated to generate the set x_{j+1} and determine the probability of accepting the model and moving on to the next step $j+1$. We assumed a Gaussian proposal distribution for all parameters of interest, with zero mean and standard deviation adjusted to explore the parameter space (Table 1). The model generated by the parameter set x_{j+1} was evaluated by computing its geophysical parameters (for example, mass and MoI) and measuring the deviations from the observations $\mathrm{d}X = X_{j+1} - X_{\mathrm{obs}}$. Evaluating a model required the definition of a probability distribution for the observations, which was assumed to be Gaussian for all the selected measurements. The probability for a given set of parameters $P(x_j)$ was then

$$P(x_j) = \exp\left(-\frac{1}{2}\,\mathrm{d}X^{\top}\Sigma\,\mathrm{d}X\right), \quad (3)$$

where Σ is the diagonal covariance matrix of the observations, with the square root of the observation uncertainties listed along the diagonal. The probability of accepting the proposed model and advancing to the next step is

$$A_{\mathrm{MH}}(x_{j+1}|x_j) = \min(1, H) = \min\left(1, \frac{P(x_{j+1})}{P(x_j)}\right), \quad (4)$$

where H is the Hastings acceptance ratio, defined by the ratio between the probability of the proposed model and the probability of the last model accepted in the chain. The model was accepted when $A_{\mathrm{MH}}(x_{j+1}|x_j)$ was larger than a sample drawn from a uniform distribution $\mathcal{U}(0,1)$. That is, H is the probability of acceptance if $H<1$. If $H>1$, which occurred when the computed observations of the proposed model were closer to the observed value than those of the last accepted model, the proposed model was always accepted. This condition allowed for a mapping of low-probability regions in the posterior distributions, thus enabling a thorough exploration of the parameter space. This process was iterated until the chain converged.

As the results may depend on the choice of the initial model, we ran 25 unique chains with different initial conditions. Once all chains had converged, resulting in ~50,000 models accepted, we discarded the first 10,000 models (burn-in) in each chain to remove the initial models, which had been randomly generated and may be significantly outside the observation distributions. We then randomly mixed the models from all the chains to obtain the final distribution of the parameters of interest. The convergence of each chain was tested according to Gelman–Rubin statistics[41], which computes the variance between the chains and the variance within them, from which a metric of convergence was built and used to check whether the observation distribution had been explored properly.

Modelling Europa's interior

Most studies in the past have assumed two- or three-layer interior models for Europa, where each layer has uniform properties throughout its depth[4,7,10]. More complex models have been elaborated by dividing the mantle into three layers, with transitions between each pair of layers at fixed depths[8]. Our analysis was based on a model of Europa that contains four material layers: a metallic core, a rocky mantle, an ocean and an ice I shell. We described the core, ocean and outer ice layer with uniform properties. The rocky mantle was modelled as a multi-layer body composed of 50 equally spaced layers. We computed the mantle pressure and density profiles based on a reference temperature profile derived from thermal evolution modelling and mineralogy calculated with Perple_X. In each inversion, the size and density of each layer (Table 1) were adjusted in our MCMC method to explore the parameter space, except for the ice-layer density, which was assumed to be the density of pure water ice at standard temperature and pressure (917 kg m^{-3})[42], and the mantle density, which was derived from the geochemical modelling. The range for each parameter was bounded to prevent the generation of physically inconsistent models. We explored configurations that may contain a metallic core by varying its radius between 0 and 1,000 km as a free parameter. The core density was allowed to vary between the density of an eutectic Fe–FeS composition (5,150 kg m^{-3}) and that of pure iron (8,000 kg m^{-3})[4].

To generate a mantle density profile that varied with depth in the MCMC, we selected a starting elemental composition and a temperature profile for each run from the outcome of the thermal evolution modelling (Supplementary Fig. 2 and Supplementary Section 1). We considered a hot profile and a colder profile. Our composition models were based on previous work by Melwani Daswani et al.[17]. Three carbonaceous chondrite compositions were assumed as precursor materials when modelling the building blocks of Europa, namely CM and CI chondrites and the MC-scale model. The latter was derived from a Monte Carlo simulation of Europa's accretion assuming preferential gravitational attraction of planetesimals in the vicinity of Europa (as the reciprocal of their squared distance from Jupiter). The resulting composition was dominated by CV chondrite material. We also included cometary compositions from Melwani Daswani and Castillo-Rogez[18], based on the properties of the comet 67P/C–G with D/I = 4 or 6. The mantle was divided into 50 sublayers of equal size. The pressure, temperature and density were computed for each sublayer (Supplementary Fig. 3). We started by computing the hydrostatic pressure at the ocean floor and assuming a temperature of 273.15 K. For each sublayer k, the pressure was calculated by assuming hydrostatic equilibrium and using the density, thickness and gravitational acceleration of the sublayer above:

$$P_k = P_{k-1} + \rho_{k-1} g_{k-1} z_{k-1}. \quad (5)$$

The temperature T_k of the sublayer was derived from the reference temperature profile using the computed pressure P_k. Diagrams of density as a function of pressure and temperature (Supplementary Fig. 4) for each precursor composition were used to compute the density ρ_k corresponding to the pressure and temperature conditions of the sublayer. This computation was iterated until the bottom of the mantle was reached, which corresponded to the core–mantle boundary

or to the centre of Europa for models without a metallic core. Once the density profile had been computed, the mass and MoI were evaluated according to equation (2).

Modelling Ganymede's interior

We constrained Ganymede's interior structure using the same technique applied to Europa to derive bounds on the mantle density and the core radius. The mass and MoI of Ganymede were derived from the analysis of radio science data acquired by Galileo (0.3105 ± 0.0028)[22]. These measurements have been updated with data from Juno, yielding a larger MoI (0.3159 ± 0.0052)[11]. We used the MoI values from both analyses (0.3105 ± 0.0028 and 0.3159 ± 0.0052) to constrain the interior models of Ganymede.

Although the relatively low pressures at the bottom of Europa's hydrosphere (~180 MPa on average from our models) prevented a phase transition to HP polymorphs, the larger pressures relevant to the hydrosphere of Ganymede makes the existence of at least one HP ice layer more probable[43,44]. Our four-layer model, therefore, accounts for a metallic core, a rocky mantle, an HP ice layer and a water-ice I outer shell. The parameter space considered in the inversion is reported in Table 1. The mantle size was derived from the radius of the moon and the sizes of the other layers. When modelling Ganymede's interior, we did not divide the water-ice I shell into an ice layer and an ocean because the latter would not have a significant impact on the interior model inversion, as its density is intermediate between those of the ice I and the HP ice layers.

Thermal evolution modelling

Our thermal evolution modelling was based on previous work applied to Iapetus[45] and Titan[46]. Heat was assumed to be transferred by thermal conduction. The evolution of the temperature T over time was computed by solving the one-dimensional diffusion equation:

$$\frac{\partial}{\partial r}\left(k(P,T)\frac{\partial T(r,t)}{\partial r}\right)+\frac{2}{r}k(T)\frac{\partial T(r,t)}{\partial r}=\rho(r)C_{\mathrm{P}}(T)\left(\frac{\partial T(r,t)}{\partial t}\right)-H(r,t), \quad (6)$$

where t is time, P is the pressure, $k(P, T)$ is the thermal conductivity, $C_{\mathrm{P}}(T)$ is the specific heat and $H(r)$ represents the heating sources (for example, radiogenic and tidal heating). The thermal profile was initialized based on accretional heating[45]:

$$T(r,t=0)=\frac{h}{C_{\mathrm{p}}(T)}\left(\frac{4}{3}\pi\rho G r^2+\frac{\langle v\rangle^2}{2}\right)+T_i, \quad (7)$$

where G is the gravitational constant, and $\langle v\rangle$ is proportional to the Safronov parameter, which ranges between 3 and 5. T_i is the temperature of the accreted material before accretion, and h is the fraction of mechanical energy dissipated as heat, which depends on the accretional process considered. We assumed cold accretion, as in Trinh et al.[16], with $h = 0.01$. To calculate the time evolution of the temperature, equation (6) was integrated by discretizing the body in layers of 2 km and using a time step of 10^4 years. We accounted for the adiabatic pressure, which was less than 30 K. Modelling of the thermophysical properties of the rock is presented in Supplementary Section 5.

Our thermal modelling focused on the evolution of the rocky mantle, such that the ice shell was not accurately treated because its evolution has little bearing on the evolution of the mantle. Convection was not modelled because its onset in the complex, depth-dependent, petrological structure described in Supplementary Fig. 10 and Supplementary Section 6 would need to be modelled, which is beyond the scope of this study. Concretely, due to mineral phase changes, the density contrast across the mantle was positive. For example, in the warmest model featured in Fig. 4, the density was 3,740 kg m^{-3} at the centre and 3,595 kg m^{-3} at the top of the anhydrous rock layer. Hence, a more complex petrological model may not favour the onset of convection compared to previous models that assumed a single type of material, although a detailed analysis should be considered in future work. Hydrothermal circulation and its role in cooling Europa's early ocean was also not accounted for. We assumed that heat transfer through thermal conduction represented an upper bound on the temperature reached in the interior.

The main heat sources that we considered were the radioactive decay of radioisotopes and tidal heating. The total specific heat production (per unit mass) at each time step $H_{\mathrm{R}}(t)$ is the sum of the heat produced by each radioactive species:

$$H_{\mathrm{R}}(t)=\sum_i^N C_{0,i}H_{0,i}e^{\frac{-ln(2)}{t_{1/2}}t}, \quad (8)$$

where $C_{0,i}$ is the initial concentration of species i, $H_{0,i}$ is the heat production per unit mass at $t = 0$ and $t_{1/2}$ is the half-life of radioisotope i. The time of formation of Europa after CAI determines the amount of short-lived radioisotopes accreted, which in turn determines the heat released shortly after accretion and largely influences the thermal evolution of the body. In particular, the estimated accretion time for Europa (~4 Myr after CAI) is about 5–6 times the half-life of ^{26}Al (7.17×10^5 years), which produces the largest heat contribution among the short-lived radioisotopes. Therefore, the contribution of ^{26}Al decay to Europa's early heat budget is substantially reduced. The main contribution to radiogenic heating is then given by long-lived radioisotopes, including ^{232}Th, ^{238}U and ^{40}K. The contribution of the latter to Europa's thermal evolution strongly depends on the amount extracted from the rocks during thermal metamorphism, which can theoretically lead to the release of almost all the potassium into the ocean[17]. In our models, we accounted for the effects of a potential potassium redistribution on Europa's radiogenic heat budget. However, we assumed small amounts of leaching (10–20%) because a fraction of the potassium released with the metamorphic fluids probably reacted with the rock while migrating upward (for example, refs. 33,47).

The other relevant heat source is tidal heating. We computed the tidal dissipation in the rocky mantle using the methodology described in Tobie et al.[48] but assuming an Andrade model as implemented in Castillo-Rogez et al.[49]. We solved the equations of motion for a body subject to self-gravitation by coupling the equilibrium equations and the Poisson equation for the gravitational potential. This resulted in a set of six ordinary differential equations, in which the unknowns were the radial functions y_i ($i = 1, \ldots, 6$) that describe the vertical and horizontal displacements and stresses and the gravitational potential. The equations were numerically integrated in the frequency domain using the correspondence principle and assuming a compressible viscoelastic rheology. The resulting radial functions were used to calculate the complex strain and stress tensors, from which the tidal heating was evaluated[48,49].

Melting of the metallic alloy and differentiation of the metallic core

The differentiation of the metallic core in a planetary body may occur following percolation of metallic alloy melt through the silicate matrix, which takes place when the temperature is above the melting point of the metallic alloy but below the solidus of the silicate matrix. We quantify here the potential of metallic core differentiation through percolation in Europa's deep interior by assuming that the core would form from iron–iron sulfide melts (Fe–FeS), over other alloys whose melting temperatures are higher (for example, Fe–FeC). To quantify the prospect for core differentiation, it is important to establish the initial composition and volumes of the sulfides. These factors determine the amount of sulfide liquid segregated from the silicate matrix, which depends on the melt volume that is produced during the thermal evolution of the moon.

The sulfides in CV chondrites consist mostly of troilite (FeS) and pentlandite $(Fe,Ni)_9S_8$, approximately in a 1:1 ratio[50]. The total volume of sulfides is 2–8 vol% (refs. 50–52). However, pentlandite was probably produced by a process occurring in the CV chondrite parent body[53]; the original sulfide condensed from the nebula was troilite[54].

Typically, it is assumed that Fe–FeS melting occurs at the eutectic temperature (~1,250 K) and then core formation begins. However, the sulfides in CV chondrites (FeS; 36 wt% S plus 64 wt% Fe) are far from the eutectic composition (24 wt% S plus 76 wt% Fe at 4 GPa), so the bulk melting temperature is higher and the volume of melt produced is correspondingly less at lower temperatures. We computed the volume of Fe–FeS melt produced during Europa's evolution by assuming that the initial composition of the sulfide was troilite, as in the CV chondrites. The melt volume as a function of pressure and temperature is shown in Supplementary Fig. 11. At the solidus temperature (~1,250 K at 4 GPa for sulfur fractions less than 36 wt%), the volume of Fe–FeS melt was small (0.1%). At 2 GPa, fully melting the sulfide required a temperature (liquidus) of 1,667 K, a situation that is never reached in our models. At 4 GPa, the highest temperature attained by our thermal evolution models (~1,800 K) led to melting of less than 50 vol% of the sulfide. We used these results to quantify the extent of Fe–FeS melting in our models and to investigate the requirements for metallic core differentiation through percolation of the dense metallic liquid. Percolation requires the establishment of a network between the metallic alloy melt pockets. Previous investigations have shown that a minimum melt volume fraction is required to achieve connectivity of these pockets (for example, refs. 55,56). This percolation threshold is highly uncertain, with values ranging from 3 to 25 vol%, depending on the sulfur content[57]. Assuming a CV chondritic composition and a percolation threshold on the lower end of the estimated range, the melting of all sulfides (~8 vol%) would lead to a higher melt volume fraction, which would trigger core differentiation through percolation. This melting would require temperatures close to the liquidus of the FeS (>1,667 K, Supplementary Fig. 11) throughout Europa's deep interior. If this condition were met in the regions with pressures larger than 2.5 GPa (radius <900 km), the entire melting of the sulfides would lead to the differentiation of a small metallic core with radius ~387 km. On the other hand, if the percolation threshold were higher than the total volume of sulfides in CV chondrites (~8 vol%), the metallic melt pockets would not be interconnected and differentiation through percolation would be prohibited.

These considerations can be applied to the outcome of our thermal evolution models. In the cold evolution scenario that we modelled, only about 10% of the volume of the mantle reached temperatures above the FeS liquidus in the warmest case modelled (without loss of potassium). Therefore, differentiation through percolation is unlikely to occur in our models because the total volume of melt would be smaller than the percolation threshold. In particular, the melt volume would be similarly small (<10 vol%) for the CI chondrites, which have smaller sulfide volumes than CV chondrites[51] despite having higher bulk sulfur concentrations[30,58], because sulfur-rich sulfides are far from the eutectic composition and, thus, require high temperatures to fully melt.

An alternative mechanism for driving the differentiation of a metallic core is through extensive melting of the rock assemblage and subsequent sinking of the denser metallic liquid (liquid–liquid segregation). For this separation to occur, temperatures in the deep interior must be raised above the solidus of the rocks. To assess the extent of rock melting in our models, we used the solidus of a bulk CV chondrite composition retrieved from experimental data obtained with the Allende meteorite[31] (Supplementary Fig. 8). Partial melting at the pressure conditions of the deep interiors of Europa (~4 GPa) and Ganymede (~8 GPa) requires temperatures above 1,690 and 1,860 K, respectively. For the maximum temperatures reached in the deep interior of the warmest model for Europa featured in Fig. 4, the molten region encompassed only about 11 vol% of the whole mantle. For 8 vol% FeS, the resulting core size was 300 km for 100 vol% melting, respectively. For a 10 wt% loss in potassium, the predicted core size was between 150 and 235 km for 25% to 100% rock melting, respectively.

Data availability

Input for the modelling and measurements are available in the published literature. The gravity measurements used in this study were retrieved from previous analyses of Galileo radio science data[4,10]. The mineralogical modelling and associated input are described in the Supplementary Information and in Melwani Daswani et al.[17]. The interior models produced in this work are available via Zenodo at https://doi.org/10.5281/zenodo.14193565 (ref. 59).

Code availability

Code relevant to the interior modelling and inversion used in this work is available upon request from the corresponding author.

References

1. Vance, S. D. et al. Investigating Europa's habitability with the Europa clipper. *Space Sci. Rev.* **219**, 81 (2023).
2. Dombard, A. J. & Sessa, A. M. Gravity measurements are key in addressing the habitability of a subsurface ocean in Jupiter's moon Europa. *Icarus* **325**, 31–38 (2019).
3. Běhounková, M. et al. Tidally induced magmatic pulses on the oceanic floor of Jupiter's moon Europa. *Geophys. Res. Lett.* **48**, e2020GL090077 (2021).
4. Anderson, J. D. et al. Europa's differentiated internal structure: inferences from four Galileo encounters. *Science* **281**, 2019–2022 (1998).
5. Zimmer, C., Khurana, K. K. & Kivelson, M. G. Subsurface oceans on Europa and Callisto: constraints from Galileo magnetometer observations. *Icarus* **147**, 329–347 (2000).
6. Schubert, G., Sohl, F. & Hussmann, H. in *Europa* (eds Pappalardo, R. T. et al.) 353–367 (Univ. Arizona Press, 2009).
7. Sohl, F., Spohn, T., Breuer, D. & Nagel, K. Implications from Galileo observations on the interior structure and chemistry of the Galilean satellites. *Icarus* **157**, 104–119 (2002).
8. Kuskov, O. L. & Kronrod, V. A. Internal structure of Europa and Callisto. *Icarus* **177**, 550–569 (2005).
9. Gao, P. & Stevenson, D. K. Nonhydrostatic effects and the determination of icy satellites' moment of inertia. *Icarus* **226**, 1185–1191 (2013).
10. Gomez Casajus, L. et al. Updated Europa gravity field and interior structure from a reanalysis of Galileo tracking data. *Icarus* **358**, 114187 (2021).
11. Gomez Casajus, L. et al. Gravity field of Ganymede after the Juno extended mission. *Geophys. Res. Lett.* **49**, e2022GL099475 (2022).
12. Genova, A. et al. Geodetic evidence that Mercury has a solid inner core. *Geophys. Res. Lett.* **46**, 3625–3633 (2019).
13. Ruesch, O. et al. Slurry extrusion on Ceres from a convective mud-bearing mantle. *Nat. Geosci.* **12**, 505–509 (2019).
14. Petricca, F. et al. Characterization of icy moon hydrospheres through joint inversion of gravity and magnetic field measurements. *Geophys. Res. Lett.* **50**, e2023GL104016 (2023).
15. Chen, M.-H. & Shao, Q.-M. Monte Carlo estimation of Bayesian credible and HPD intervals. *J. Comput. Graph. Stat.* **8**, 69–92 (1999).
16. Trinh, K. T., Bierson, C. J. & O'Rourke, J. G. Slow evolution of Europa's interior: metamorphic ocean origin, delayed metallic core formation, and limited seafloor volcanism. *Sci. Adv.* https://doi.org/10.1126/sciadv.adf3955 (2023).
17. Melwani Daswani, M., Vance, S. D., Mayne, M. J. & Glein, C. R. A metamorphic origin for Europa's ocean. *Geophys. Res. Lett.* **48**, e2021GL094143 (2021).

18. Melwani Daswani, M. & Castillo-Rogez, J. C. Porosity-filling metamorphic brines explain Ceres's low mantle density. *Planet. Sci. J.* **3**, 21 (2022).
19. Desch, S. J., Kalyaan, A. & Alexander, C. M. The effect of Jupiter's formation on the distribution of refractory elements and inclusions in meteorites. *Astrophys. J.* **238**, 11 (2018).
20. Connolly, J. A. D. Computation of phase equilibria by linear programming: a tool for geodynamic modeling and its application to subduction zone decarbonation. *Earth Planet. Sci. Lett.* **236**, 524–541 (2005).
21. Connolly, J. A. D. The geodynamic equation of state: what and how. *Geochem. Geophys. Geosyst.* https://doi.org/10.1029/2009GC002540 (2009).
22. Anderson, J. D., Lau, E. L., Sjogren, W. L., Schubert, G. & Moore, W. B. Gravitational constraints on the internal structure of Ganymede. *Nature* **384**, 541–543 (1996).
23. Kivelson, M. G. et al. Discovery of Ganymede's magnetic field by the Galileo spacecraft. *Nature* **384**, 537–541 (1996).
24. Schubert, G., Zhang, K., Kivelson, M. G. & Anderson, J. D. The magnetic field and internal structure of Ganymede. *Nature* **384**, 544–545 (1996).
25. Kivelson, M. G., Khurana, K. K. & Volwerk, M. The permanent and inductive magnetic moments of Ganymede. *Icarus* **157**, 507–522 (2002).
26. Anderson, J. D., Jacobson, R. A., Lau, E. L., Moore, W. B. & Schubert, G. Io's gravity field and interior structure. *J. Geophys. Res.: Planets* **106**, 32963–32969 (2001).
27. Mousis, O. et al. Early stages of Galilean moon formation in a water-depleted environment. *Astrophys. J. Lett.* **944**, L37 (2023).
28. Borlina, C. S., Weiss, B. P., Bryson, J. F. & Armitage, P. J. Lifetime of the outer Solar System nebula from carbonaceous chondrites. *J. Geophys. Res.: Planets* **127**, e2021JE007139 (2022).
29. Barr, A. C., Citron, R. I. & Canup, R. M. Origin of a partially differentiated Titan. *Icarus* **209**, 858–862 (2010).
30. Palme, H., Lodders, K. & Jones, A. in *Planets, Asteroids, Comets and The Solar System* 2nd edn (ed. Davis, A. M.) 15–36 (Elsevier, 2014).
31. Agee, C., Li, J., Shannon, M. & Circone, S. Pressure-temperature phase diagram for the Allende meteorite. *J. Geophys. Res.: Solid Earth* **100**, 17725–17740 (1995).
32. Hussmann, H. & Spohn, T. Thermal-orbital evolution of Io and Europa. *Icarus* **171**, 391–410 (2004).
33. Néri, A., Guyot, F., Reynard, B. & Sotin, C. A carbonaceous chondrite and cometary origin for icy moons of Jupiter and Saturn. *Earth Planet. Sci. Lett.* **530**, 115920 (2020).
34. Malhotra, R. Tidal origin of the Laplace resonance and the resurfacing of Ganymede. *Icarus* **94**, 399–412 (1991).
35. Showman, A. P. & Malhotra, R. Tidal evolution into the Laplace resonance and the resurfacing of Ganymede. *Icarus* **127**, 93–111 (1997).
36. Batygin, K. & Morbidelli, A. Formation of giant planet satellites. *Astrophys. J.* **894**, 143 (2020).
37. Mazarico, E. et al. The Europa Clipper gravity and radio science investigation. *Space Sci. Rev.* **219**, 30 (2023).
38. Kivelson, M. G. et al. The Europa Clipper magnetometer. *Space Sci. Rev.* **219**, 48 (2023).
39. Khurana, K. K., Kivelson, M., Hand, K. P. & Russel, C. T. in *Europa* (eds Pappalardo, R. T. et al.) 571–586 (Univ. Arizona Press, 2009).
40. Metropolis, N., Rosenbluth, A. W., Rosenbluth, M. N., Teller, A. H. & Teller, E. Equation of state calculations by fast computing machines. *J. Chem. Phys.* **21**, 1087–1092 (1953).
41. Gelman, A. & Rubin, D. B. Inference from iterative simulation using multiple sequences. *Stat. Sci.*https://doi.org/10.1214/ss/1177011136 (1992).
42. Marshall, S. J. *The Cryosphere* (Princeton Univ. Press, 2011).
43. Sotin, C. & Tobie, G. Internal structure and dynamics of the large icy satellites. *Comptes Rendus Phys.* **5**, 769–780 (2004).
44. Journaux, B. et al. Large ocean worlds with high-pressure ices. *Space Sci. Rev.* https://doi.org/10.1007/s11214-019-0633-7 (2020).
45. Castillo-Rogez, J. et al. Iapetus' geophysics: rotation rate, shape, and equatorial ridge. *Icarus* **190**, 179–202 (2007).
46. Castillo-Rogez, J. C. & Lunine, J. I. Evolution of Titan's rocky core constrained by Cassini observations. *Geophys. Res. Lett.* https://doi.org/10.1029/2010GL044398 (2010).
47. Soder, C. & Romer, R. Post-collisional potassic-ultrapotassic magmatism of the Variscan orogen: implications for mantle metasomatism during continental subduction. *J. Petrol.* **59**, 1007–1034 (2018).
48. Tobie, G., Mocquet, A. & Sotin, C. Tidal dissipation within large icy satellites: applications to Europa and Titan. *Icarus* **177**, 534–549 (2005).
49. Castillo-Rogez, J. C., Efroimsky, M. & Lainey, V. The tidal history of Iapetus: spin dynamics in the light of a refined dissipation model. *J. Geophys. Res.: Planets* https://doi.org/10.1029/2010JE003664 (2011).
50. Malissa, H., Hermann, F., Kluger, P. & Kiesl, W. Chemical and microprobe investigations of the Allende-meteorite. *Microchim. Acta* **60**, 434–450 (1972).
51. Bland, P. A., Cressey, G. & Menzies, O. N. Modal mineralogy of carbonaceous chondrites by X-ray diffraction and Mössbauer spectroscopy. *Meteorit. Planet. Sci.* **39**, 3–16 (2004).
52. Howard, K., Benedix, G., Bland, P. & Cressey, G. Modal mineralogy of CV3 chondrites by X-ray diffraction (PSD-XRD). *Geochim. Cosmochim. Acta* **74**, 5084–5097 (2010).
53. Brearley, A. J. Origin of graphitic carbon and pentlandite in matrix olivines in the Allende meteorite. *Science* **285**, 1380–1382 (1999).
54. Larimer, J. W. & Anders, E. Chemical fractionations in meteorites. II. Abundance patterns and their interpretation. *Geochim. Cosmochim. Acta* **31**, 1239–1270 (1967).
55. Bagdassarov, N., Golabek, G., Solferino, G. & Schmidt, M. Constraints on the Fe-S melt connectivity in mantle silicates from electrical impedance measurements. *Phys. Earth Planet. Inter.* **177**, 139–146 (2009).
56. Solferino, G. F. D., Thomson, P.-R. & Hier-Majumder, S. Pore network modeling of core forming melts in planetesimals. *Front. Earth Sci.* https://doi.org/10.3389/feart.2020.00339 (2020).
57. Néri, A., Guignard, J., Monnereau, M., Toplis, M. & Quitté, G. Metal segregation in planetesimals: constraints from experimentally determined interfacial energies. *Earth Planet. Sci. Lett.* **518**, 40–52 (2019).
58. Lodders, K. & Fegley, B. *The Planetary Scientist's Companion* (Oxford Univ. Press, 1998).
59. Petricca, F., Castillo-Rogez, J., Genova, A., Styczinski, M., Cochrane, C. & Vance, S.. Supplementary material for Petricca et al. 2024 'Partial differentiation of Europa and implications for the origin of materials in the Jupiter system'. *Zenodo* https://doi.org/10.5281/zenodo.14193565 (2024).

Acknowledgements

We thank F. Nimmo (University of California Santa Cruz), C. Glein (Southwest Research Institute), O. Mousis (Aix-Marseille Université), H. Hussmann (DLR), R. Malhotra (University of Arizona) and the Europa Clipper Gravity/Radio Science investigation team for fruitful discussions and suggestions that substantially improved the manuscript. F.P. and A.G. acknowledge funding from the Italian Space Agency (Contract 2021-19-HH.0). M.M.D. was supported by NASA's Habitable Worlds programme (Solicitation NNH18ZDA001N-HW, Proposal No. 18-HW18_2-0111). This work was partially supported by 22-PSIE22_2-0024 and by NASA's Europa Clipper mission. Parts of this work were carried out at the Jet

Propulsion Laboratory, California Institute of Technology, under a contract with NASA (80NM0018D0004). M.J.S. was supported by an appointment to the NASA Postdoctoral Program at the Jet Propulsion Laboratory, California Institute of Technology, administered by Oak Ridge Associated Universities under a contract with NASA (80HQTR21CA005).

Author contributions

F.P., J.C.C.-R. and A.G. conceived the initial study. F.P. designed and performed the interior structure inversion and analysis. J.C.C.-R. contributed the thermal evolution modelling and analysis. M.M.D. provided the mineralogy and geochemical modelling. All authors contributed to the discussion and interpretation of the results. F.P. and J.C.C.-R. wrote the first draft of the paper. All authors contributed to the revisions of the paper.

Competing interests

The authors declare no competing interests.

Additional information

Supplementary information The online version contains supplementary material available at https://doi.org/10.1038/s41550-024-02469-4.

Correspondence and requests for materials should be addressed to Flavio Petricca.

Peer review information *Nature Astronomy* thanks Stefano Bertone and the other, anonymous, reviewer(s) for their contribution to the peer review of this work.